

LIQUID FLOW DISTRIBUTION IN CATALYTIC DISTILLATION COLUMNS : USE OF HIGH ENERGY X-RAY TOMOGRAPHY

Saïd Aferka, University of Liège, Liège, Belgium
Anil Saroha, Indian Institute of Technology, Delhi, New Delhi, India
Dominique Toye, University of Liège, Liège, Belgium
Pierre Marchot, University of Liège, Liège, Belgium
Michel Crine, University of Liège, Liège, Belgium

Abstract

This work focuses on the use of X-ray tomography to investigate the liquid flow distribution in a structured catalytic distillation packing. The experimental setup is made up of a 4 m high and 0.1 m inner diameter transparent PVC column. The packed bed (1.8 m high - 0.1 m diameter) is constituted by the superposition Mellapak™ 752Y and Katapak™-SP12 packing elements. These latter are filled with non prewetted non porous glass beads. The tomographic set-up is composed of a high energy X-ray constant potential generator (max. 420 kV) and a linear array detector of 1280 photodiodes, which corresponds to a spatial resolution at the centre of the object of approx. 360 µm. Cross sections of the liquid hold up distribution are obtained at various column heights for different liquid flow rates. The repartition of the liquid hold up between baskets and corrugated sheets is quantified. Wall wipers and column wall effects are visualized.

Introduction

Catalytic distillation is a type of process intensification that utilizes close coupling of separation and chemical reaction systems. The combination of heterogeneously catalysed chemical reactions and distillation in one single apparatus has several advantages. Such a hybrid process offers the potential for large savings of capital, energy, materials and significant reduction of waste products that satisfies the increasing demand for sustainable technology (Noeres *et al.*, 2002). Various catalyst packing configurations based on a regular alternation of zones with weak permeability (catalytic zones) and of high permeability (liquid and vapour transport zones) have been reported in the literature (see e.g., van Hasselt *et al.*, 1999, Ratheesh *et al.*, 2004). These sandwich structures allow postponing the flooding beyond usual operating flowrates.

However, designing catalytic distillation columns remains a challenge (Adler *et al.*, 2000; Olujic *et al.*, 2003; Schmit and Eldridge, 2004). The introduction of separation and reaction zones in one single apparatus leads to complex interactions between hydrodynamics, vapour-liquid equilibrium, vapour-liquid mass transfer, internal diffusion and chemical kinetics. Different models of the process as well as new structured catalytic packings have been developed. However, to take advantage of these potentialities requires a better understanding of complex multiphase flow phenomena occurring in catalytic distillation packings. The knowledge of hydrodynamics imposed by the internal configuration is vital but seems lacking in the open literature (Behrens, 2006).

X-ray tomography has been shown to be an efficient non-intrusive tool to see inside and to adequately image the liquid and vapour flow distribution in packed columns (Toye *et al.*, 1998). In this paper, we report on the use of a high energy and high resolution X-ray tomograph able to penetrate through stainless steel packings and dense catalytic zones and to achieve a spatial resolution of a few hundreds of microns.

Materials & Methods

The X-ray tomography set-up

The tomographic set-up is illustrated in Fig.1. The generator is a Baltograph CSD450 constant potential generator (Balteau NDT, BE). It may be operated between 30 and 420 kV. The X-ray source (S) is an oil cooled, bipolar TSD420/3 tube (Comet, CH and Balteau NDT, BE), producing a 40° aperture fan beam. Its minimum focus size is 0.8x0.8 mm following norm IEC336 - EN12543. Its intensity may be varied between 2 and 8 mA depending on the voltage used. A lead collimator produces a 1 mm thick fan beam.

The detector (D) is a X-Scan 0.4f2-512-HE (Detection Technology, FI). It is constituted by a linear array of 1280 photodiodes each coupled with a CdWO₄ scintillator. The detector is 512 mm long with a 0.4 pixel pitch, which corresponds to a spatial resolution at the centre of the object of approx. 360 µm. The integration time may be set from 0.67 to 15 ms and its dynamic range is 12 bits.

The mechanical rig designed by Pro Actis (BE) is constituted by two parts, a source-detector arm (A) and a rotating table (R) on which is fixed the object to be scanned. The arm is a very rigid metallic structure on which are embedded the X-ray source and the detector. This arm is embedded to a carriage (C) which slides following two vertical high precision machined rails. The carriage vertical displacement is obtained with a great accuracy by an helicoidal screw (V) rotated by a synchronous motor equipped with frequency variator. The high voltage cable is connected to the source (S) via a folding cable channel (B).

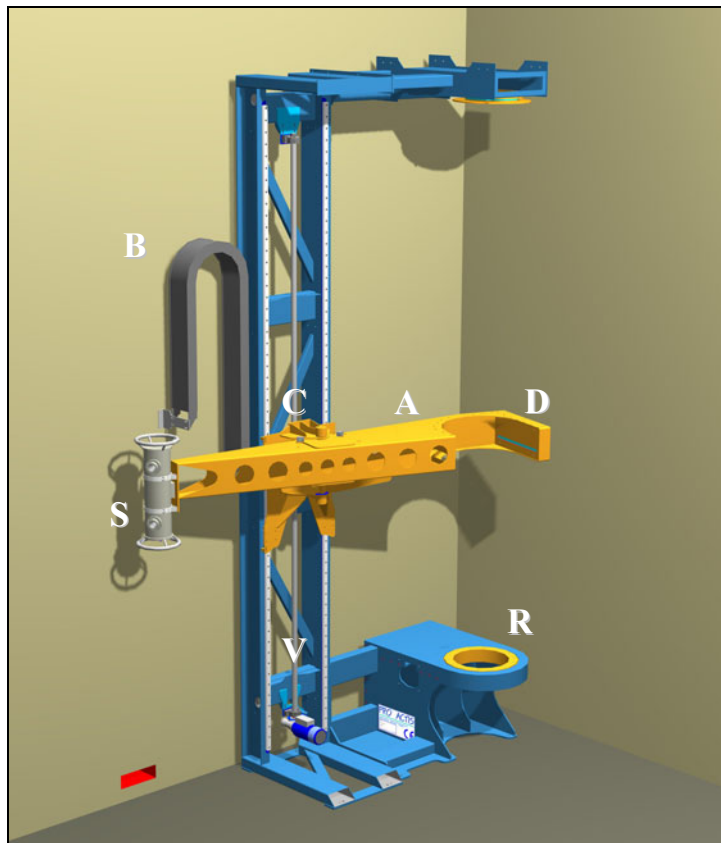


Figure 1

X-ray tomographic setup.

**A: arm; B: folding cable channel; C: carriage;
D: detector bank; R: rotating table; S: X-ray source; V: helicoidal screw**

The test rig allows manipulation of rather large objects (max. height: 4m, max. diam: 0.45 m). During the tomographic measurements, the column rotates slowly around its vertical axis, while the X-ray source and the detector remain fixed. The entire scanning unit is located inside a room surrounded by 0.6 m thick concrete walls to prevent exposing operating personnel to X-ray radiation.

The column to be scanned is fitted on the rotating table, the rotation of which is obtained by a synchronous motor equipped with frequency variator which is supervised by the data acquisition system. This test rig allows a vertical movement up to 3780 mm keeping verticality and horizontality errors within 1 mm. Further details on the X-ray tomographic facility as well as on the control system are provided elsewhere (Toye *et al.*, 2005). More views of this set-up are available at http://www.ulg.ac.be/bioreact/equip_tomoX_420kV.htm

Reconstruction of object cross sections are obtained by a classical linear back projection algorithm adapted to the fan beam geometry implemented in the Fourier domain. In order to eliminate the background noise affecting reconstructed images, thresholding using the method of Otsu (implemented in the Matlab 7 Image Processing Toolbox 4.2) is applied. This thresholding is applied only to the pixels located inside the external wall of the column obtained using image masking. Reconstructed sections are squares of 499x499 pixels and the spatial resolution in the plane is around 360 μm .

Packing elements

The column used in this study has a height of 4 m. and an inner diameter of 0.1 m. It is made of transparent PVC. The packing (1.6 m high - 0.1 m diameter) is constituted by the superposition of, from the top to the bottom, 3 Mellapak™ 752Y, 4 Katapak™-SP12 and 1 Mellapak™ 752Y packing elements. These packings are manufactured by Sulzer Chemtech, CH. They are made of stainless steel. Mellapak™ 752Y packing elements (see illustration in Fig. 2) are composed of 0.2 mm thick stainless steel corrugated sheets that are ± 1 mm embossed and perforated with 4 mm holes. These sheets are tightened together by two metallic wire gauze wall wipers. The geometric characteristics are presented in Table 1.

Table 1 : Mellapak™ 752Y (Sulzer Chemtech) geometric characteristics

Packing element height	0.2 m
Packing element diameter	0.09 m
Specific surface area	510 m^2/m^3
Packing void fraction	97.5 %
Corrugation angle	41 °
Corrugation base	9.85 mm
Corrugation height	6.50 mm

Table 2 : Katapak™ SP12 (Sulzer Chemtech) geometric characteristics

Packing element height	0.2 m
Packing element diameter	0.09 m
Specific surface area	236 m^2/m^3
Packing void fraction	82 %
Catalyst void fraction	24 %
Ratio of number of reaction section to number of separation section	1:2

Suffix 12 in Katapak™ SP12 denotes an alternative arrangement of two corrugated sheets (separation zone) and one catalyst basket (reaction zone), see illustration in Fig. 3. Catalyst baskets are made of wire gauze and are filled by 1 mm non prewetted glass beads. The bottom and the top of each basket is closed by tapering the wire gauze. Baskets and sheets are tightened together by three equidistant metallic wire gauze wall wipers. The corrugated sheets are similar to those used in Mellapak™ 752Y packings. The geometric characteristics of the packing are presented in Table 2 (Ratheesh and Kannan, 2004).



Figure 2
View of a Mellapak™ 752Y packing element



Figure 3
Top view of one Katapak™ SP12 packing element

Results & Discussion

Dry packing visualization

Tomographic measurements have been realised in about 40 packing cross sections, separated by 0.04 m, i.e., both through Mellapak and Katapak packing elements. Figs. 4a and 4b (grey level images) illustrate two 2D reconstructed sections of the Mellapak™ 752Y packing. Scales are in pixels of 0.36 mm width. Details of sheet corrugations (embossements, holes) are visible on these images.

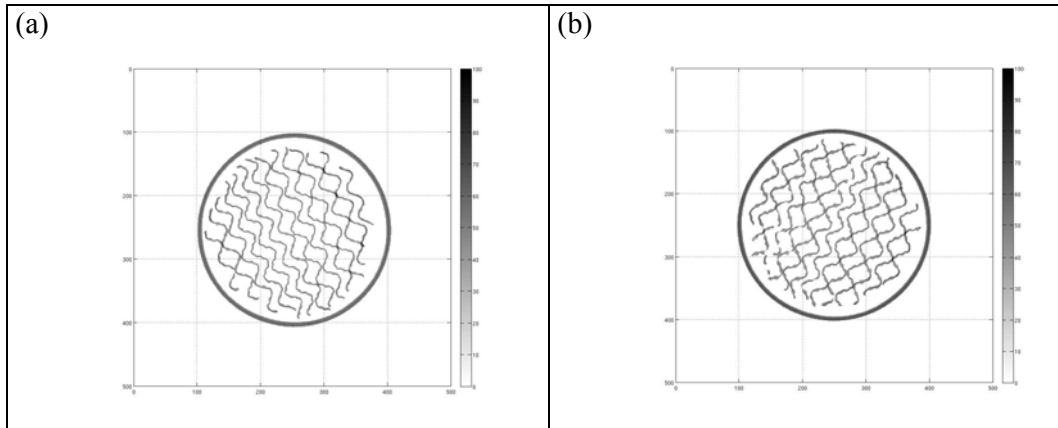


Figure 4 : 2D reconstructed images in a Mellapak™ 752Y metallic structured packing

Figs. 5a and 5b (grey level images) illustrate two 2D reconstructed sections (scales are in pixels of 0.36 mm width) of the Katapak™ SP12, scanned at a two different height around the middle of an element. All the packing details (corrugated sheets embossed and perforated, catalyst baskets, ...) are clearly visible. However, the small glass beads, within the baskets, are not completely resolved. The cross sections illustrated in Fig. 5a is scanned at the level of one of the 3 wall wipers surrounding each Katapak element. Fig. 5b crosses corrugated sheets at the level of perforations.

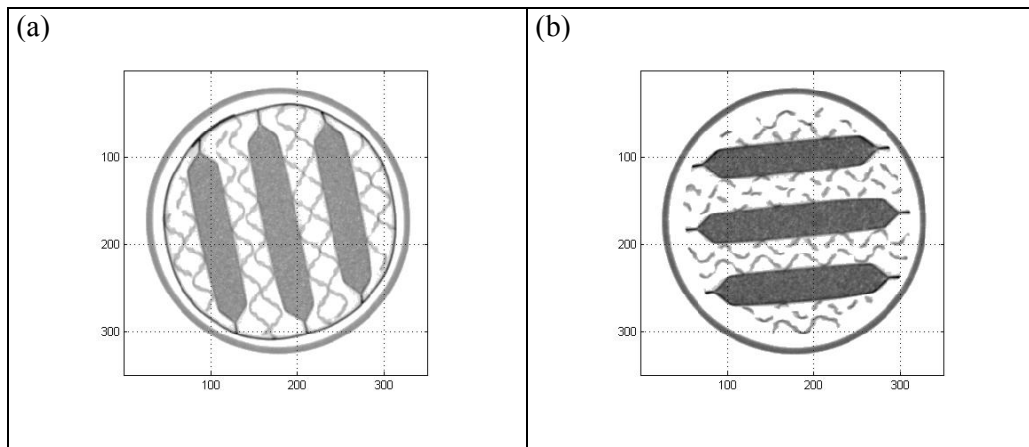


Figure 5 : 2D reconstructed images in a Katapak™ SP12 metallic structured packing

Liquid holdup distribution

A multiple point source (approx. 1000 drip points/m²) distributor was used to feed the liquid at the top of the column. The superficial velocities of the liquid and gas phases ranged between 10 and 50 m³/m².h and 0.5 and 2 m/s, respectively.

Figs. 6a and 6b illustrate liquid distributions observed in two cross sections of Mellapak 752Y elements situated in the top and bottom layers of the column, i.e., at 0.33 m and 1.65 m below the feeding point, respectively. The liquid superficial velocity equals 12 m³/m².h. These two colour images are obtained by superimposing the binary images of the liquid distribution (in blue) on the binary images of dry packing (in grey). To obtain the sole liquid contribution, the projection data obtained on the dry column are subtracted, before reconstruction, from those obtained at the same height on the irrigated column.

The liquid is roughly uniformly distributed within the two cross-sections. The liquid follows closely sheet corrugations, with a texture of films and rivulets. The packing wetting is not complete. Films and rivulets seem to thicken after passing through the Katapak elements, as illustrated by comparing Figs. 6a and 6b.

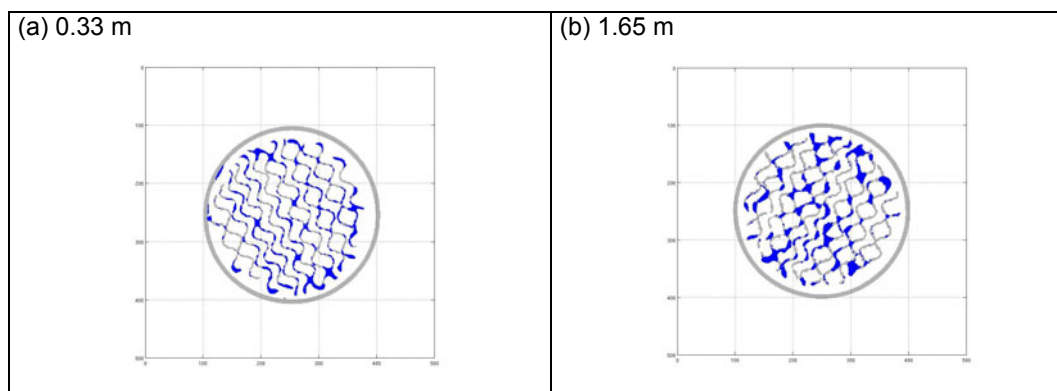


Figure 6 :
Liquid distribution in a cross sections situated at 0.33 m and 1.65 m
below the liquid feed point.
Mellapak™ 752Y ; Liquid superficial velocity = 12 m³/m².h
Gas superficial velocity = 0 m/s

Figs. 7 and 8 present a series of Katapak™-SP12 packing cross sections at various column heights separated by 4 cm for a liquid superficial velocity of 47 m³/m².h. These two colour images are still obtained by superimposing the binary images of the liquid distribution (in blue) on the binary images of dry packing (in grey).

Fig. 7 illustrates liquid distribution observed above and within the uppermost packing element. Fig. 7a illustrates the liquid distribution 2 cm above the Katapak element, i.e., in the lower part of the Mellapak element. The liquid is roughly uniformly distributed, as already observed in Fig. 6a.

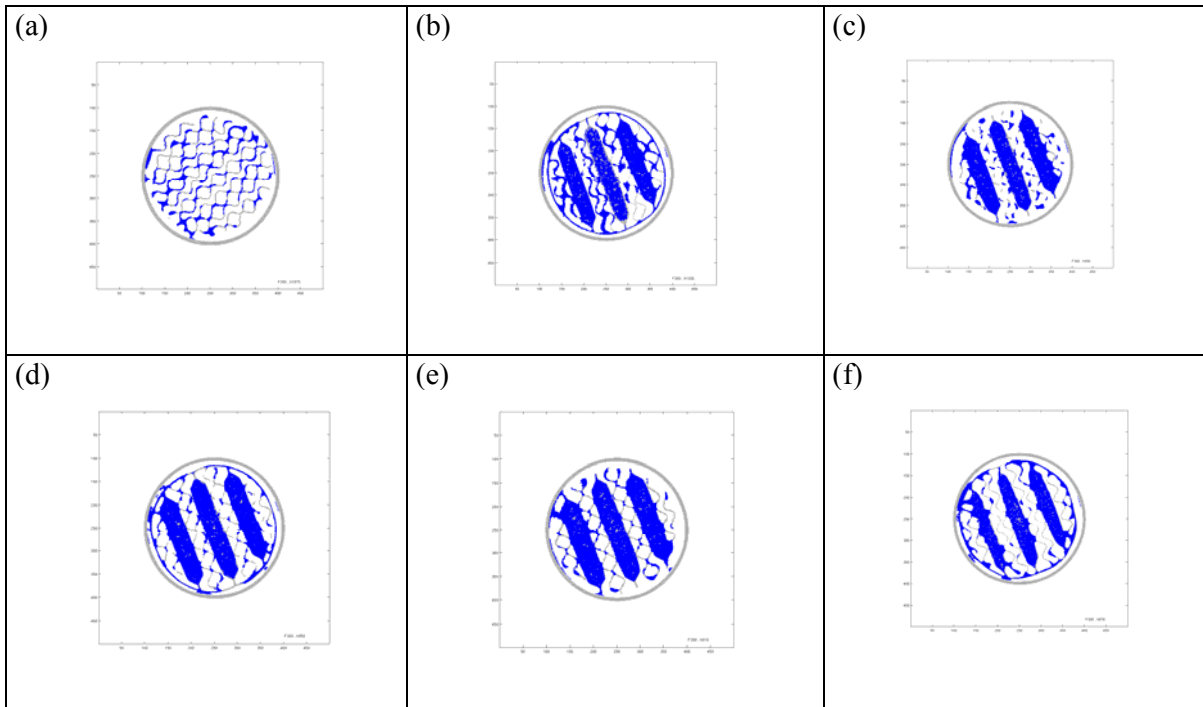


Figure 7

Liquid distribution in several cross sections situated above and within the upper Katapak™ SP12 packing element
Liquid superficial velocity = $47 \text{ m}^3/\text{m}^2 \cdot \text{h}$; Gas superficial velocity = 0 m/s

Fig. 7b illustrates the liquid distribution 2 cm from the top the upper Katapak element, i.e., in the entrance zone. One clearly observes baskets are almost completely flooded with liquid, while a significant part of the liquid still, roughly evenly distributed, trickles over the corrugated sheets.

When moving down through the packing element (Figs 7c to 7f), liquid is progressively captured within the baskets. The wetting of the corrugated sheets is significantly reduced. Each packing element is surrounded by 3 wall wipers that can be observed in Figs 7b, 7d and 7f. They collect liquid trickling over the column wall and redirect it towards the inside the structured packing.

Figs. 8a to 8e illustrate liquid distribution observed in different cross sections, separated by 4 cm, within the second Katapak element from the top. Fig. 8f illustrates liquid distribution observed 2 cm below this element, i.e., at the entrance of the third Katapak element. One still observes a decrease of the wetting of the corrugated sheets when moving down through the packing: liquid is still progressively captured by the baskets. However, liquid is less evenly distributed within these baskets especially within the central one.

One possible explanation seems to be an uneven distribution of liquid leaving the upper baskets, due to some irregularities in the basket closing. The resulting maldistribution is most probably exacerbated by the poor wettability of the dry, non prewetted glass beads filling baskets. The same phenomenon is still observed, to a less extent, at the entrance of the third Katapak element (Fig. 8f).

Visual observations illustrated by Figs. 7 and 8 can be confirmed and quantified by reporting the total liquid holdup versus the packing height at different increasing liquid superficial velocities : 12, 24 and $47 \text{ m}^3/\text{m}^2 \cdot \text{h}$. Fig. 9 plots the liquid hold-up at cross section levels separated by 4 cm. All experimental points are located within the elements and not in between the elements. As expected, the total liquid hold up increases with the liquid velocity.

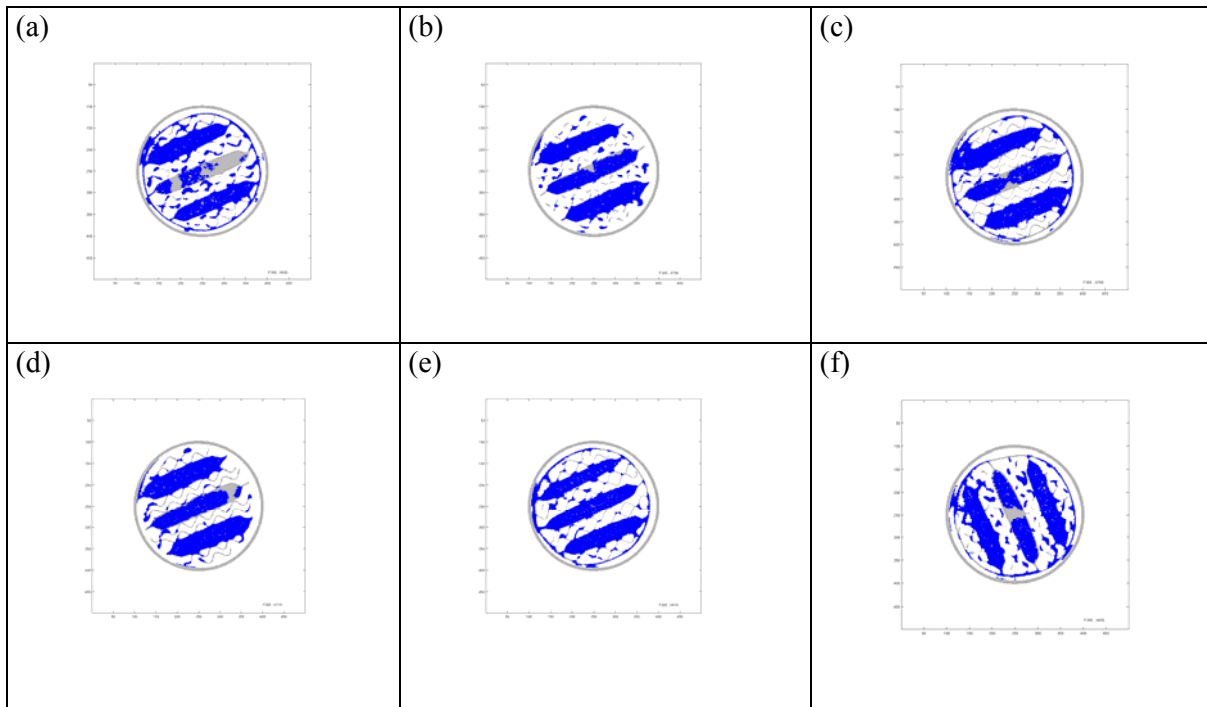


Figure 8

Liquid distribution in several cross sections situated within and below the second uppermost Katapak™ SP12 packing element
Liquid superficial velocity = $47 \text{ m}^3/\text{m}^2 \cdot \text{h}$; Gas superficial velocity = 0 m/s

Moving from the top of the bed, at the right side of the graph, the total liquid hold up within each Katapak element increases first, then decreases as the end of the element is reached. The maximum hold up for each element is located around its middle height.

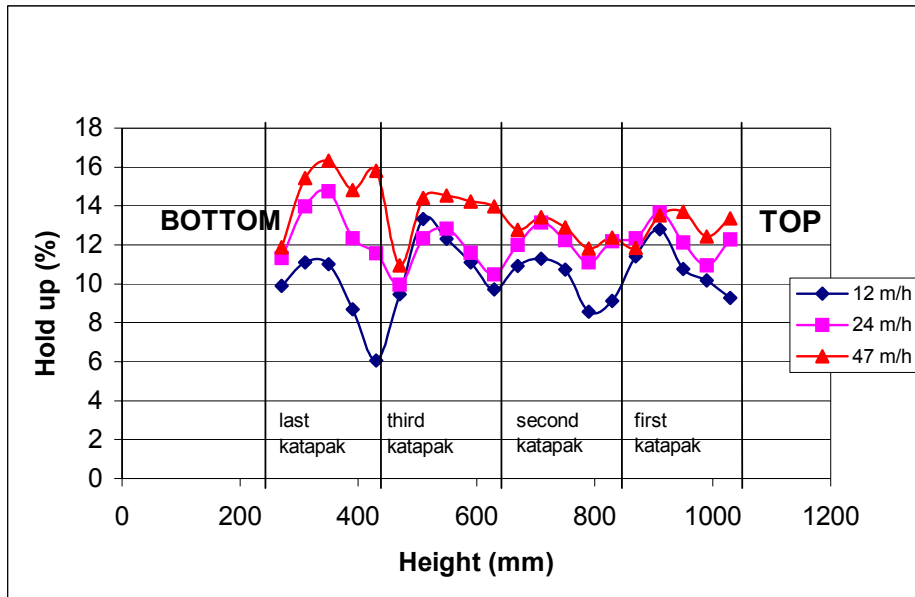


Figure 9

Total liquid holdup versus the packing height
at three different liquid superficial velocities : $12, 24$ and $47 \text{ m}^3/\text{m}^2 \cdot \text{h}$
(gas velocity: 0 m/s)

The distribution of liquid among the central and outermost baskets can be determined by applying a mask corresponding to the cross section of each basket. These masks are determined on dry packing images.

Fig. 10 shows the total liquid hold up inside the two outermost baskets as a function of the height in the column for the three investigated liquid superficial velocities : 12, 24 and 47 m³/m² h. At the two highest liquid velocities, the liquid hold up remains almost constant along the column height, close to the packing void fraction: baskets are almost completely flooded. Results observed at the lowest liquid velocity, i.e. 12 m³/m² h differ strongly from the others. The liquid holdup decreases significantly at most of the junctions between Katapak elements.

In Fig. 11 , the total liquid hold up of the central basket, seems to vary strongly with its vertical location. Variations are larger for the smallest liquid velocity (12 m/h). These variations confirm the maldistribution phenomenon observed in Fig. 8.

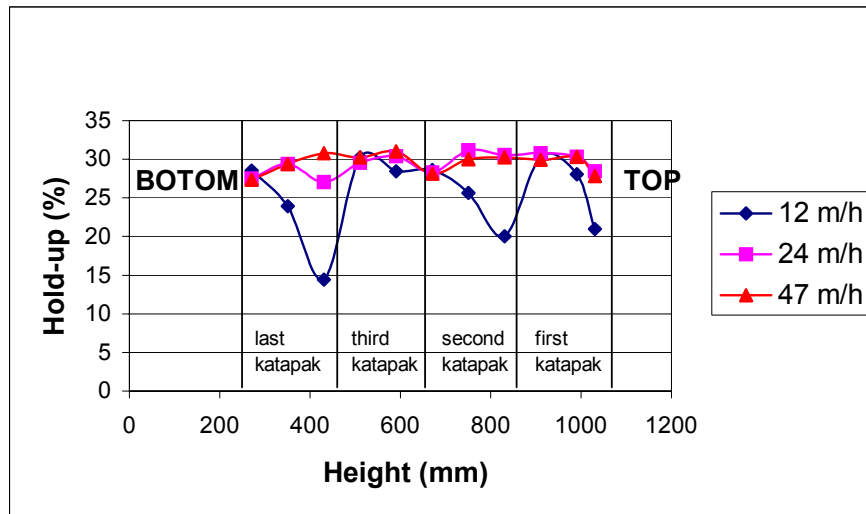


Figure 10
Total liquid holdup inside outermost baskets versus the packing height at three different liquid superficial velocities : 12, 24 and 47 m³/m² h (gas velocity: 0 m/s)

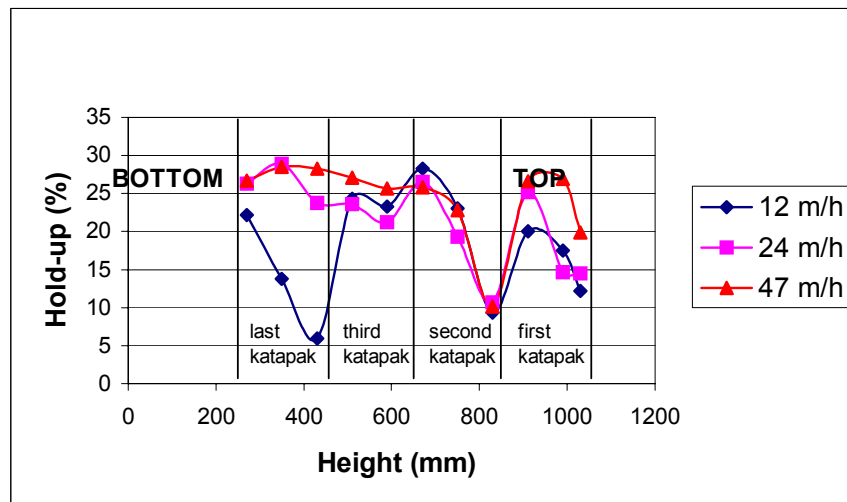


Figure 11
Total liquid holdup inside central baskets versus the packing height at three different liquid superficial velocities: 12, 24 and 47 m³/m² h (gas velocity: 0 m/s)

Fig. 12 shows the fraction of total liquid hold up present inside the baskets. It is almost independent of the liquid superficial velocity. It fluctuates between 60 and 80%, passing through minima at the junction between packing element. This confirms a large part of the liquid holdup is inside baskets as visualized by Figs. 7 and 8.

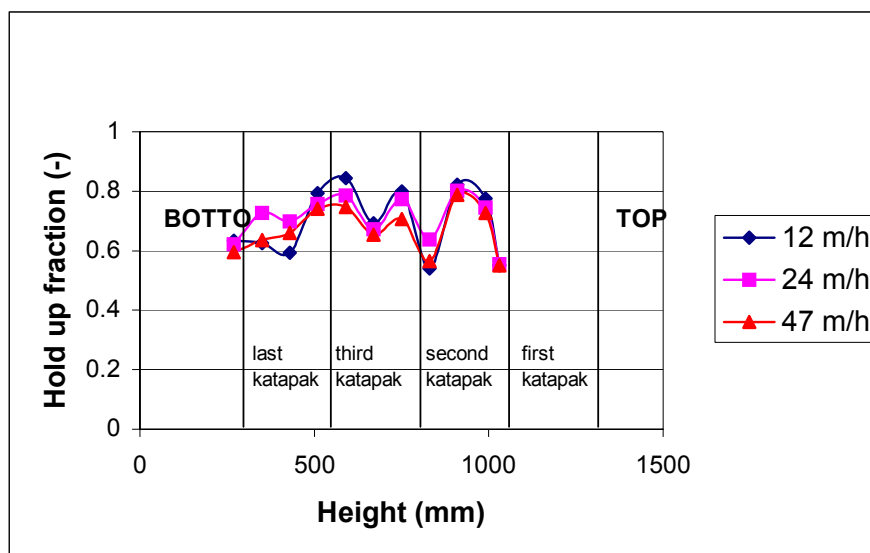


Figure 12
Total liquid hold up fraction inside the baskets versus the packing height at three different liquid superficial velocities: 12, 24 and 47 m³/m² h (gas velocity: 0 m/s)

Conclusions

The X-ray imaging results reported in this paper are preliminary results. They indicate the technique has significant potential to provide insight into gas-liquid hydraulics prevailing in complex catalytic distillation metallic packings. This information should greatly assist on-going efforts to develop fundamentally rigorous hydraulic models.

Acknowledgements

This work was performed in the frame of a research financed by the Belgium's French Community (research contract ARC 05/10-334). The authors also thank the National Fund for Scientific Research (FNRS, Belgium) for their financial support. A.Saroha is indebted to the FNRS for a temporary position of Postdoctoral Researcher. Packing elements used in this research were kindly provided by Sulzer Chemtech, CH.

References

1. Adler, S., Beaver, E., Bryan, P., Robinson, S., Watson, J. (2000), Vision 2020 - Separations Roadmap, American Institute of Chemical Engineers, New York.
2. Behrens, M. (2006), Hydrodynamics and Mass Transfer Performance of Modular Catalytic Structured Packing, PhD Thesis, ISBN 13:978-90-9020347-8, TU Delft.
3. Noeres, C., Hoffmann, A., Górak, A. (2002), Reactive distillation : Non-ideal flow behaviour of the liquid phase in structured catalytic packings, *Chemical Engineering Science*, 57, pp. 1545-1549.

4. Olujic, Z, Frey, G., Jansen, H., Kaibel, B., Rietfort, T., Zich, E. (2003), Distillation column internals related process intensification developments, Proceedings of the Sixth Italian Conference on Chemical and Process Engineering, June 2003, Pisa (Italy), in *Chemical Engineering Transactions*, 3, pp. 367-372.
5. Ratheesh, S., Kannan, A. (2004), Holdup and pressure drop studies in structured packings with catalysts, *Chemical Engineering Journal*, 104, pp. 45-54.
6. Schmit, C.E., Eldrige, R.B. (2004), Investigation of X-ray imaging of vapor-liquid contactors. I. Studies involving stationary object and a simple flow system, *Chemical Engineering Sciences*, 59, pp. 1255-1266.
7. Toye, D., Marchot, P., Crine, M., Pelsser, A-M., L'Homme, G. (1998), Local measurements of void fraction and liquid holdup in packed columns using X-ray computed tomography, *Chemical Engineering and Processing*, 37, pp. 511-520.
8. Toye, D., Crine, M., Marchot, P. (2005), Imaging of liquid distribution in reactive distillation packings with a new high energy X-ray tomograph, *Measurement Science and Technology*, 16, pp. 2213-2220.
9. van Hasselt, B, Calis, H., Sie, S., van den Bleek, C. (1999), Liquid holdup in the three-levels-of-porosity reactor, *Chemical Engineering Science*, 54, pp. 1405-1411.